Carboxyl group (–CO2H) functionalized coordination polymer nanoparticles as efficient platforms for drug delivery.

Fernando Novio,* [a,b] Julia Lorenzo,[c] Fabiana Nador,[a] Karolina Wnuk[a,b] and Daniel Ruiz-Molina [a,b]

[a] Dr. F. Novio, Dr. F. Nador, K. Wnuk, Dr. D. Ruiz-Molina
Institut Català de Nanociència i Nanotecnologia (ICN2)
Edifici ICN2, Campus UAB
Cerdanyola del Vallès, 08193(Spain)
Fax: (+ 34) 937372648
E-mail: fnovio@cin2.es

[b] Dr. F. Novio, K. Wnuk, Dr. D. Ruiz-Molina
Consejo Superior de Investigaciones Científicas (CSIC)
Edificio ICN2, Campus UAB
Cerdanyola del Vallès, 08193(Spain)

[c] Dr. J. Lorenzo
Departament de Bioquímica i de Biologia Molecular.
Institut de Biotecnologia i Biomedicina (IBB).
Universitat Autònoma de Barcelona
Cerdanyola del Vallès, 08193(Spain)

Abstract

Functionalization of nanoparticles can significantly influence their properties and potential applications. Although researchers can now functionalize metal, metal oxide or organic polymer nanoparticles with a high degree of precision, controlled surface functionalization of nanoscale coordination polymer particles (CPPs) has remained a significant research challenge. This lack of methodology is perhaps one of the greatest roadblocks to the advancement of CPPs into high added-value drug delivery applications. Here we report having achieved this goal through stepwise formation and functionalization protocol. We fabricated robust nanoparticles with enhanced thermal and colloidal stabilities by incorporation of carboxyl group and the surface carboxyl groups can be subsequently functionalized through well-known peptide coupling reactions. The set of chemistries that we employed as proof-of-concept enabled a plethora of new functional improvements for the application of CPPs as drug delivery carriers, including enhanced colloidal stabilities and the incorporation of additional functional groups such as PEG or fluorescent dyes that enabled tracking of their cellular uptake. Finally, we ascertained the cytotoxicity of the new CPP nanoparticles loaded with camptothecin to human breast adenocarcinoma (MCF-7). Efflux measurements show that the encapsulation of camptothecin enhances the potency of the drug in 6.5-fold and increases the drug retention within the cell.

Introduction

Miniaturization of coordination polymers (CPs)[1] to the nanoscale represents a novel class of highly customizable functional particles for drug-delivery on combining the rich diversity, chemistry and properties of coordination complexes to the advantages of nanomaterials.[2] Metal-organic frameworks (MOFs) have already been successfully used with this aim; MOFs allow control over the release cargo via modification of tunable pores with an exceptionally high surface area and therefore loading capacity. The crystalline nature of MOFs facilitates analyses of host–guest interactions and systematic drug encapsulation and release studies, as well as theoretical models.[3] In addition to MOFs, amorphous nanoscale coordination polymer particles (CPPs) have recently emerged as an effective alternative for the use of coordination polymer as drug delivery carriers. Since first being reported less than a decade ago,[4] nanoscale CPPs have already shown their efficacy as encapsulation carriers,[5] sensors,[6] biopolymers,[7] drug delivery,[8] or theranostics[9] platforms. Nonetheless, the synthetic methodology for CPPs is in its fledgling stage. To date, there have not been any reports of methods to systematically control the surface functionality of CPPs or to master their modification at the nanoscale. This lack of methodology is perhaps one of the greatest roadblocks to the advancement of CPPs into high added-value medical applications. This is especially relevant for drug delivery applications, where significant advances involve the development of nanoparticles with specific surface functions and/or recognition chemicals that allow for an enhanced biological activity, imaging or stability. Although functionalization of metal or metal oxide,[10,11] MOFs [12] or pure organic polymer nanoparticles [13] can be achieved with a high degree of precision, this new family of metal-organic coordination polymer particles remained unexplored.

The most direct approach to achieve this goal is a priori the hierarchical assembly of nanoparticles using ligands with the desired functional group, a small fraction of which is expected to remain on the nanoparticle surface. However, this approach is limited by the unpredictable interplay of supramolecular interactions between ligands according to its chemical composition, steric constraints and bulk material properties, all of which can influence the final composition, stability and morphology of the nanoparticles. Thus, we envisioned the use of ligands bearing a reactive group that enables reproducible fabrication of nanoscale platforms and their post-synthetic modification. With this aim, herein we report the fabrication of CPPs incorporating ligands containing carboxyl groups (Figure 1 top), which have been shown to reinforce both the chemical and colloidal stability of the nanoparticles. Moreover, the surface carboxylates can be transformed into myriad functionalities through well-known condensation reactions, as schematically shown in Figure 1 down. The plethora of functionalities added range from polyethyleneglycol (PEG) to the incorporation of fluorescent dyes enabling tracking of their cellular uptake. Finally, we ascertained the successful cytotoxicity of the new CPP nanoparticles loaded with camptothecin to human breast adenocarcinoma cells (MCF-7). Efflux measurements showed a 6.5 fold increase in antitumoral activity of the encapsulate drug in comparison with free drug. This represents a notable evidence of the potential utility of these CPPs as chemotherapeutic nanomedicines with high uptake and in vitro activity under low dosing regimen.

In a typical experiment, an aqueous solution of $M(CH_3COO)_2 \cdot xH_2O$ (where M stands for cobalt or iron) was added to an ethanolic solution combining two co-ligands: 3,4-dihydroxycinnamic acid (dhc), used to introduce the carboxylic acid group on the structure, and 1,4-bis(imidazol-1-ylmethyl)benzene (bix), used as a counter ligand to induce polymerization. After vigorous stirring at room temperature a pale brown greenish precipitate was obtained for the cobalt complex (**CPP0-Co**) and a dark brown one for the iron sample (**CPP0-Fe**). The precipitate was then collected by centrifugation, washed several times with ethanol and dried under vacuum. SEM and TEM images revealed spherical nanoparticles with an average diameter of 110±17nm (**CPP0-Co**) or 94±11 nm (**CPP0-Fe**) (see Figure 2), as confirmed by dynamic light scattering (DLS). We were also able to control the average size by simply regulating the stirring rate (see Supporting Information S1). The reaction conditions were adjusted to assure a particle mean size close to 100 nm, an optimal range to be applied as drug delivery systems.[14] The chemical analysis data agreed with the general chemical formula $[M(dhc)_2(bix)]_n$. X-ray Powder Diffraction data showed the typical pattern for an amorphous material. Fourier-transform infrared (FT-IR) spectra evidenced the coordination of the bix and catechol ligands to the metal and the permanence of the acidic group. Energy-Dispersive X-ray Spectroscopy confirmed the presence of the metal (Co or Fe) and of carbon, oxygen and nitrogen (see Supporting Information S2).

Chemical and colloidal stability. Surface carboxylic groups already enable control on the colloidal dispersion in water mainly by electrostatic repulsions, as already shown for different families of inorganic nanoparticles.[15] Zeta-potential measurements on **CPP0-Co** and **CPP0-Fe** in aqueous buffer (~20 mM) at neutral pH (pH 7.3) gave values of –25.0 ± 8.2 mV and –34.3 ± 9.7 mV, respectively. The resulting colloidal suspensions are stable for a few days. From here, the surface charge can be tuned by simply adjusting the pH of the buffer (see Figure 2e-f)—a feature which has been harnessed in other families of nanoparticles to modulate properties such as colloidal stability, toxicity and biocompatibility.[16] For instance, a pH increase to 9.0 led to a more negative zeta-potential value of -57.7 ± 6.2 mV (**CPP0-Co**) and -61.2± 5.1 mV (**CPP0-Fe**) and consequently, to less particle aggregation and therefore, more stable dispersions during several weeks due to an increase in Coulombic repulsions (increasing the pH further, to ~12.0, resulted in chemical decomposition as evidenced by a yellowish solution containing particles of inconsistent sizes). Contrariwise, decreasing the pH from 7.3 to 4.2 induced protonation of most of the surface carboxylate groups, leading to a zeta-potential value close to zero. Accordingly, the CPPs were highly prone to aggregate, which ultimately led to their precipitation. Interestingly, this aggregation and precipitation is reversible: bringing the pH back up enabled recovery of the stable colloidal suspension. Finally, when the pH was decreased to below 3.0 the CPPs rapidly decomposed.

Combined TGA/DSC and SEM experiments also evidence a considerable enhancement of the thermal and chemical stability most likely due to the formation of several hydrogen bonds within the core of the nanoparticle. **CPP0-Co** and **CPP0-Fe** nanoparticles begin to melt over 105 ºC and decompose over 220 ºC, well over those found for other CPP families. For comparison purposes, model **CPP1-Co** nanoparticles obtained by replacement of dhc ligands by 3,4-di(tert-butyl) catechol groups were also studied. As expected, introduction of bulky

tert-butyl groups without having the possibility to induced hydrogen bonds induces a decrease in the melting point down to ca. 60 ºC (see Supporting Information S2). Such difference in thermal stability can be translated to chemical robustness. Whereas **CPP0** nanoparticles are stable in water or PBS solution for several weeks, those of CPP1 remain only for a few days.

Functionalization of CPP0 with the 6-aminofluorescein (ANF) fluorescent dye. First attempts to couple the surface carboxyl groups of **CPP0-Fe** and **CPP0-Co** were done with a 6-aminofluorescein dye in a water/ethanol solution at room temperature. After 24 h, stable **ANF/CPP0-Fe** and **ANF/CPP0-Co** nanoparticles were isolated without any morphological change concerning initial **CPP0-Co** (figure 3a). Successful coupling was indicated by the FTIR spectra; FT-IR spectrum lacked the characteristic NH_2 stretching/bending bands (at 3500-3350 and 1700-1500 cm^{-1}) of the amine group from ANF and exhibited a less intense carboxylic acid C-OH stretching band (at 1300 cm^{-1}) due to the carboxyl-amino surface coupling. The signal corresponding to the formation of the amide group is barely distinguishable, however, characteristic signals from 6-aminofluorescein are observed. (see Supporting Information S3). Fluorescence measurements on **ANF/CPP0-Fe** and **ANF/CPP0-Co** revealed that the nanoparticles display a strong green luminescence (emission peak centered at ca. 520 nm) upon excitation at 490 nm, both in solution and in solid state (Figure 3b). Such excitation is characteristic of the ANF group, though coordinative bonding induces its maximum absorbance to shift upon partial hybridization with the metal ion (see Supporting Information S3). In contrast, under identical conditions, **CPP0-Fe** and **CPP0-Co** did not emit any fluorescence. The concentration of ANF on the CPPs surface was calculated by absorbance measurements (see Experimental Section) taking as reference the absorbance spectra of the corresponding non-functionalized nanoparticles. This calculation was not conclusive in the case of **ANF/CPP0-Fe**, however for **ANF/CPP0-Co** a concentration of $1.58 \cdot 10^{-9}$ mol ANF per mg of nanoparticles was calculated.

Cellular uptake of NPs. After functionalization with the fluorescent dye, we then monitored the uptake of the fluorescently labeled **ANF/CPP0** nanoparticles in MCF-7 cells using confocal laser scanning microscopy (CLSM). After 24 h of incubation, orthogonal views of CLSM images (Figure 3c, X Z) clearly exhibited the localization of these nanoparticles inside the cells. In contrast, no fluorescence was detected in untreated (control) cells. The cellular uptake of these nanoparticles was also investigated quantitatively. MCF-7 cells were incubated with **ANF/CPP0-Co** (100 μg/mL) or **ANF/CPP0-Fe** (100 μg/mL) for 24 h, and then lysed in PBS-1% SDS. The fluorescently labeled CPPs inside of the cells were quantified by analyzing the cell lysate in a spectrofluorometer reader (extinction wavelength: 490 nm; emission wavelength: 520 nm). The relative cellular internalization of **ANF/CPP0-Co** was 27%, and of fluorescently labeled **ANF/CPP0-Fe**, 39%. Transport mechanism of CPPs through the cell membrane is not known yet; though most likely it takes place through a endocytosis pathway, consistent with reports on anionic carboxylated and hydroxyl terminated PAMAM dendrimers.[17] This should be the case of our negatively charged particles at physiological pH (7.4).

Functionalization of CPP0 with polyethylene glycol (PEG). We also coupled the surface carboxyl groups of CPPs to amino-functionalized NH_2-PEG chains (O-(2-aminoethyl)polyethylene glycol 3,000) in a phosphate buffer solution (pH 7.4). The reaction afforded a colloidal suspension, which was centrifuged, and then washed several times with an ethanol/diethyl ether solution. The resulting **PEG/CPP0-Fe** and **PEG/CPP0-Co** solid was dried under vacuum. Successful coupling was indicated by the FTIR spectra of (see Supporting Information S4). As observed by SEM (Figure 4a-b), the new **PEG/CPP0-Fe** and **PEG/CPP0-Co** nanoparticles are 8 to 10% larger than the corresponding precursors **CPP0-Fe** and **CPP0-Co** and exhibit a 15% larger hydrodynamic radius based on DLS measurements, which we attributed to the presence of the PEG groups. Moreover, the surface charge can be also tuned by simply adjusting the pH of the buffer. For **PEG/CPP0-Fe**, increasing the pH to 9.0 led to a decrease in zeta-potential (from -11.4 mV to -22.3 mV) and consequently, to less particle aggregation in water (Figure 4c) —a feature which has previously been exploited for **CPP0-Fe** and **CPP0-Co**. More interesting is the comparison of colloidal dispersions of **PEG/CPP0** and non-functionalized **CPP0** nanoparticles at different concentrations in a PBS phosphate buffer (1mg/mL and 5mg/mL). After 1 week the solutions containing **CPP0-Fe** nanoparticles had undergone notable sedimentation, whereas the **PEG/CPP0-Fe** dispersions remained much more stable, owing to the PEG groups (figure 4d). Finally, the surface concentration of PEG groups was determined by ^{1}H-NMR measurements (see Experimental Section). For this the integral ratios of PEG methylene protons obtained upon dissolution of the **PEG/CPP0-Fe** nanoparticles is compared with a calibration curve of blank PEG methylene protons measured at different concentrations resulting in a value of $8.42 \cdot 10^{-3}$ mg ($2.80 \bullet 10^{-9}$ mol) of PEG per mg of nanoparticles, and a surface concentration of PEG chains around ~13 pmol/cm^2 (35% of the theoretical surface carboxyl groups; see Experimental Section). If compare the calculated PEG concentration with the corresponding ANF concentration in the surface of analogous CPPs we observed as increasing of 1.7 times the amount of PEG related to ANF. This difference can be due to different factors such as coupling reactivity, steric hindrance or others. Further studies will be necessary to elucidate the main factors that govern it.

Cytotoxicity measurements. In order to investigate the cytotoxicity of the different nanoparticles on the MCF-7 breast cancer cells XTT assay was used. MCF-7 cells were treated during 24h with increasing doses of Fe and Co nanoparticles and the results indicate that MCF-7 cells retained more than 75% viability, in comparison with untreated cells, even at high nanoparticle concentrations (see Supporting Information S5). It could be suggested that the chemical composition of the nanoparticles and the low percentage of metal ions (less than 10% in mass) did not contribute to toxicity. Thus, nanoparticles showed no cytotoxicity and thus great potential to be drug carriers.

Encapsulation and drug delivery. To evaluate de effectiveness of these nanoplatforms as nanocarriers and their therapeutic potential as drug delivey systems for cancer treatment, **CPP0-Fe** nanoparticles were used to encapsulate campothecin (CPT). By addition of an aqueous solution of $Fe(CH_3COO)_2$ to an ethanolic solution containing the mixture bix/dhc and the drug ([CPT] = 3.0 x 10^{-3} M) under stirring at room temperature, the resulting

nanoparticles (**CPT@CPP0-Fe**) were obtained. Afterwards the nanoparticles were purified by centrifugation and washed several times with ethanol. This process was repeated until no fluorescence signal from non-encapsulated CPT was detected in the supernatant solution by fluorimetric measurements. Representative SEM and TEM images reveal the formation of the nanoparticles with a mean size of 112±19 nm and the entrapment of CPT was confirmed by both absorption and fluorescence measurements (Figure 5); encapsulation efficiency of ca. 80% and drug loading capacity up to 18% in weight were obtained by absorption measurements with respect to the initial drug concentration used, and comparison with non-loaded blank nanoparticles.

Under these conditions, the half maximal inhibitory concentration (IC50) for **CPT@CPP0-Fe** was 2.79 ng and 1.16 ng CPT/ml, at 24h and 72h, respectively. The cytotoxicity effect of the free CPT in a MCF7 cellular culture at 24 h and 72 h under the same experimental conditions was also studied for comparison purposes. The half maximal inhibitory concentration (IC50) was 18.52 and 7.37 ng/ml at 24h and 72h, respectively. This represents an astonishing 6.5-fold drug efficacy increase upon encapsulation (Figure 5d). These excellent results have been attributed to higher intracellular levels of CPT arising from an increased cellular uptake of the drug upon encapsulation.

Extrapolation to other compositions. Finally, to demonstrate that our new synthetic framework can be extrapolated to other reactive groups opening the possibility to systematically tune CPPs performance for drug delivery, we fabricated CPP platforms with ligands bearing a reactive aldehyde group. Following the methodology previously described but replacing the 3,4-dihydroxycinnamic acid (dhc) by the 3,4-dihydroxybenzaldehyde (dhba) ligand, amorphous spherical nanoparticles with an average diameter of 100±12 nm (**CPP2-Fe**) were obtained as confirmed by combined SEM, DLS experiments and X-ray Powder Diffraction experiments. Fourier-transform infrared (FT-IR) spectra evidenced the coordination of the bix and catechol ligands to the metal and the permanence of the aldehyde group. Energy-Dispersive X-ray Spectroscopy confirmed the presence of the metal (Fe) and of carbon, oxygen and nitrogen. Afterwards we coupled the surface aldehyde groups of **CPP2-Fe** to a 1-Pyrenebutyric hydrazide (PBH) dye in a ethanolic solution, in presence of acetic acid and heating at 80ºC. After 6 h, stable **PBH/CPP2-Fe** nanoparticles were isolated without any morphological change concerning initial CPP2. Successful coupling was indicated by the FTIR spectra (see Supporting Information S6).

Fluorescence measurements on **PBH/CPP2-Fe** revealed that the nanoparticles display a strong luminescence (emission peak centered at ca. 410 nm) upon excitation at 347 nm, both in solution and in solid state, confirming the validity of our approach.

Conclusion

We fabricated robust nanoparticles by incorporation of carboxyl groups. The resulting nanoscale CPP exhibit three main advantages: I) they offer a highly robust platform

reinforced by several supramolecular hydrogen bonds within the polymeric network, while retaining the morphological characteristics and encapsulation capacities, II) surface carboxyl groups allow for the systematic control over the colloidal dispersion of CPPs and III) the surface carboxylates can be transformed into myriad functionalities through well-known peptide coupling reactions, which is difficult to achieve by direct formation. This has been demonstrated via labeling with new bioactive functional groups (fluorescent dyes or PEG**).**

We have also explored their use as drug delivery carriers. **CPT@CPP0-Fe** nanoparticles have shown a 6.5-fold increase efficacy with respect to the free CPT, affording formulations with low clinically relevant IC50s. Moreover, the relatively high load capacity of drugs such as CPT, their low cytotoxicity, the possibility to image the cell internalization by functionalization with fluorescent groups and the control of colloidal stability in aqueous dispersions provide very promising and non-developed nanoplatforms with applications on drug delivery.

Experimental Section

Experimental Solvents and starting materials were purchased from Sigma-Aldrich and used as received, without further purification, unless otherwise stated. 1,4-Bis(imidazol-1-ylmethyl)benzene (bix) [18] and **CPP1-Co** nanoparticles [19] were synthesized according to a previously reported methods.

Synthesis of **CPP0-Co** and **CPP0-Fe**. 1,4-Bis(imidazol-1-ylmethyl)benzene (59 mg, 0.25 mmol) and 3,4-dihydroxycinnamic acid (dhc, 90 mg, 0.5 mmol) were dissolved in 15 mL of ethanol. Under vigorous stirring (800 rpm) the solution was treated with an aqueous solution of either $Co(CH_3COO)_2 \bullet 4H_2O$ (62.3 mg, 0.25 mmol in 2 mL H_2O; for **CPP0-Co**) or $Fe(CH_3COO)_2$ (43.5 mg, 0.25 mmol in 2 mL H_2O; for **CPP0-Fe**), which turned it either brownish-green or dark blue, respectively, and led to rapid form ation of a precipitate. After the solution was stirred at room temperature for 30 minutes, the precipitate was collected by centrifugation, and then washed with ethanol several times. The solvent was removed and the solid was dried under vacuum. SEM and TEM images of the resulting spherical nanoparticles showed a size distribution of 110±17 nm and 94±11 nm for **CPP0-Co** and **CPP0-Fe** respectively. C,H,N analysis (%) calcd for $C_{32}H_{28}O_8CoN_4$: C 58.63, H 4.31, N 8.55; found: C 59.34, H 4.79, N 8.18. C,H,N analysis (%) calcd for $C_{32}H_{28}O_8FeN_4$: C 58.91, H 4.33, N 8.59; found: C 59.48, H 4.92, N 8.40. FT-IR (ATR) CPP0-Co: ν =3412.5 (s), 3092.4 (s), 1615.3 (s), 1585.2 (s), 1486.2 (m), 1396.4 (m), 1088.2 (m), 809.9 (m), 727.7 (m), 658.21 (m) cm-1. FT-IR (ATR) CPP0-Fe: ν = 3422.1 (s), 3101.3 (s), 1609.7 (s), 1478.6 (m), 1395.3 (m), 1095.4 (m), 798.9 (m), 722.5 (m), 657.3 (m) cm-1.

Synthesis of CPP2-Fe. 1,4-Bis(imidazol-1-ylmethyl)benzene (59 mg, 0.25 mmol) and 3,4-dihydroxybenzaldehyde (69 mg, 0.5 mmol) were firstly dissolved in 15 mL of ethanol. Under vigorous stirring (800 rpm), the solution was treated with an aqueous solution of $Fe(CH_3COO)_2$ (43.5 mg, 0.25 mmol in 2 mL H_2O), which turned it light brown and led to

rapid formation of a precipitate. After the solution was stirred at room temperature for 30 minutes, the precipitate was collected by centrifugation, and then washed with ethanol several times. The solvent was removed and the solid was dried under vacuum. SEM and TEM images of the resulting spherical nanoparticles showed a size distribution of 100±12 nm. C,H,N analysis (%) calcd for $C_{28}H_{24}O_6FeN_4$: C 59.17, H 4.26, N 9.86; found: C 59.49, H 4.35, N 10.01; FT-IR (ATR): ν =2361.2 (m), 2335.3 (m), 1651.7 (m), 1570.6 (m), 1483.2(s), 1434.4 (m), 1282.5 (s), 1102.5 (m), 948.4 (w), 821.4 (m), 750.3 (m), 640.1 (m) cm-1.

Synthesis of CPT@CPP0-Fe nanoparticles. These drug loaded spheres were obtained by addition of an aqueous solution (5 ml) of $Fe(CH_3COO)_2$ (109 mg, 0.625 mmol) to an ethanolic solution (25 ml) containing a mixture of bix (147.5 mg, 0.625 mmol), dhc (225 mg, 1.25 mmol) and the drug CPT (3.0 x 10-3 M) under vigorous stirring at room temperature. The resulting encapsulated metal-organic polymer nanoparticles were purified by centrifugation and washed at least three times with ethanol to eliminate impurities and rest of the drug adsorbed on the nanoparticles surface. The encapsulated systems were dried and storage under inert atmosphere in the freeze. These nanoparticles are easily redispersable in different organic solvents, water or phosphate buffer.

Functionalization of CPP0-Co/Fe CPPs with 6-aminofluorescein (ANF): To a stirring dispersion of 30 mg of nanoparticles in 15 mL of H_2O/EtOH (4:1) were added 5 mg (0.014 mmol) of 6-aminofluorescein. After 10 minutes, EDC (10 mg, 0.05 mmol) and NHS (5.75 mg, 0.06 mmol) were added, and the mixture was stirred at room temperature for 6 hours. The resulting particles were purified by centrifugation, and then washed with ethanol several times to remove any excess starting material (the total absence of any remaining, non-attached dye in the supernatant solution was confirmed by the absence of any fluorescence signal). The precipitate was dried under vacuum overnight.

Functionalization of CPP2-Co/Fe CPPs with 1-Pyrenebutyric hydrazide (PBH): To a stirring dispersion of 8 mg of nanoparticles in 6 mL of ethanol were added 3 mg (0.017 mmol) of 1-Pyrenebutyric hydrazide and one drop of acetic acid. The mixture was stirred at 80ºC for 8 hours. The resulting particles were purified by centrifugation, and then washed with water and ethanol several times to remove any excess of starting material (the total absence of any remaining, non-attached dye in the supernatant solution was confirmed by the absence of any fluorescence signal). The precipitate was dried under vacuum overnight.

Functionalization of CPP0-Co/Fe CPPs with *O*-(2-aminoethyl)polyethylene glycol 3.000 (NH_2-PEG). Carboxyl-functionalized CCPs (30mg) were dispersed in 10 mL of phosphate buffer solution (PBS, 50 mM, pH 7.4). Subsequently, to activate the carboxylic acid groups, EDC (20 mg, 0.10 mmol) and NHS (11.5 mg, 0.13 mmol) were added at room temperature and the solution was kept for 2 h under continuous stirring. Afterwards, 100 mg of PEG prepared in 5 mL of PBS were added and the solution was stirring for 24 h at room temperature. The resulting nanoparticles were collected by centrifugation, washed with water and ethanol, and dried under vacuum.

Characterization: Optical microscopy images were obtained with an Axio Observer Z-1 (Zeiss) inverted optical microscope, equipped with an XY motorized sample holder. The light source is a high-pressure Hg steam lamp of short arc (HBO 103/2 of 100W). The microscope is equipped with different objectives (5x, 10x, 20x, 50x, 100x) as well as filters for fluorescence measurements (DAPI: exc. BP 365/12, emis. LP 397; Alexa Fluor 488: exc. BP 450, emis. LP 515; and Alexa Fluor 546: exc. BP 540/12, emis. LP 590). Fluorescence was detected with an AxioCam HRc camera with a Sony CCD sensor (resolution: 1388 x 1040 pixels = 1.4 Mpxl). SEM measurements were performed with a HITACHI S-570 operating at 15 kV. The samples were prepared by drop casting of the corresponding dispersion on aluminum tape followed by evaporation of the solvent under room conditions. Before analysis the samples were metalized with a thin layer of gold, using a sputter coater (Emitech K550). Transmission electron microscopy (TEM) images were acquired with a Jeol JEM-1400 microscope operating at 120 kV. The samples were prepared by casting a drop of the corresponding sample dispersion on a holey carbon copper grid, and then evaporating off the solvent under room temperature. Size distribution and surface charge of the nanoparticles were measured by DLS, using the Zetasizer Nano 3600 instrument (Malvern Instruments, UK), whose size range limit is 0.6 nm to 6 μm (5 nm to 10 μm for zeta-potential). Note: the diameter measured by DLS is the hydrodynamic diameter. The samples comprised aqueous dispersions of the nanoparticles in distilled water or in buffer. All samples were diluted to obtain an adequate nanoparticle concentration. The data reported are mean values for each sample, which were measured in quadruplicate. To study the influence of pH on zeta-potential, the nanoparticles were dispersed in different PBS buffers (pH: 4.2, 7.3, 9.0 or 12.0). The IR spectra have been recorded using a Tensor 27 (Bruker) spectrophotometer equipped with a single-reflection diamond window ATR accessory (MKII Golden Gate, Specac). Powder XRD spectra were recorded at room temperature on a high-resolution texture diffractometer (PANalytical X'Pert PRO MRD) equipped with a Co-Kα radiation source (λ = 1.7903Å) and operating in reflection mode. The solid samples were placed in an amorphous silicon oxide flat plate and measured directly.

Determination of ANF concentration on CPPo nanoparticles. The concentration of ANF on the surface was calculated using a solution containing 2 mg of **ANF/CPP0** nanoparticles in 3ml of PBS by applying the Beer's Law ($c = A / \varepsilon\ l$); specifically molar extinction coefficient for 6-aminofluorescein εANF = 83,000. The absorbance signal of the attached ANF was obtained by deconvolution the spectra of the functionalized nanoparticles taking as reference the absorbance spectra of the corresponding non-functionalized nanoparticles. This calculation was easy for **ANF/CPP0-**Co nanoparticles, however the high dispersion of the particles and broad signal of ANF in **ANF/CPP0-Fe** make difficult to obtain a good result (see Supporting Information S3). Once the ANF concentration in the dispersion is calculated, the amount of fluorescent dye per mg of nanoparticles can be easily calculated. For **ANF/CPP0-Co**: [ANF]calc = $1.06 \cdot 10^{-6}$ M; that match with $1.58 \cdot 10^{-9}$ mol ANF per mg of nanoparticles.

Determination of attached PEG groups by ^{1}H-NMR. In a sample experiment, 20 mg of dry **PEG/CPP0-Fe** nanoparticles was re-dispersed in deuterated methanol. Two drops of

deuterated hydrochloric acid were added to the solution to afford the complete dissolution and demetalation of the coordination polymer. ^{1}H-NMR spectra (250 MHz) were recorded on a Bruker Avance DRX-250 spectrometer with chemical shifts and integration relative to an external reference. The external reference consisted of 10 μL acetone dissolved into 0.5 mL of deuterated methanol in a WILMAD coaxial insert tube immersed in the 5 mm NMR sample tube (acetone chemical shift: 2.15 ppm). For the calibration curve, NH_2-PEG (MW 3000) with different known weights was dissolved in deuterated methanol, and the samples were characterized by NMR. The calibration curve was obtained by plotting the integral ratios of the PEG methylene protons (chemical shift: 3.25-3.60 ppm) against the external reference signal (see Supporting Information S7). By measuring the integral ratios of PEG methylene protons obtained from the dissolution of the coordination polymer respect to the same external reference, the average PEG concentration was obtained by comparison of the results with the calibration curve. The calculations afford an amount of $9.42 \cdot 10^{-3}$ mg of PEG per mg of nanoparticles. The calculated surface area of the particles was then used to determine the surface concentration of PEG. By modeling the nanoparticles as perfect spheres of 100 nm size containing one –COOH group each ~170Å^2 that correspond to the metal-metal separations in typical Co-bix complexes (between 12-14Å), as extracted from different structural characterizations found in literature.[20] Thus it is possible to give an estimate of the expected maximum coverage of the surface by the PEG chains. So, this theoretical approximation affords a maximum concentration of carboxyl groups on the nanoparticles surface around ~38 pmol/cm^2. With the known surface area of the particles used, the surface concentration of PEG can be determined accordingly.[21] The calculated surface concentration of PEG obtained was ~13 pmol/cm^2 This translates to a functionalization level of 34% of the initial surface carboxyl groups, which is consistent with the estimated value (ca. 40%) obtained from zeta-potential studies by comparison of PEG functionalized and nonfunctionalized nanoparticles (see Supporting Information S7).

Cytotoxicity assay. Human breast-cancer cells (MCF-7) were obtained from American Type Culture Collection (ATCC, Manassas, VA, USA). The cells were routinely cultured with DMEM F12 (Invitrogen) containing 10% heat-inactivated fetal bovine serum (FBS), at 37 ºC in a humidified (5%) CO_2 atmosphere. The cytotoxicity of each type of nanoparticle was evaluated by the XTT (sodium 2,3,-bis(2-methoxy-4-nitro-5-sulfophenyl)-5-[(phenylamino)-carbonyl]-2H-tetrazolium inner salt) assay. MCF-7 cells were plated at a density of 5 x 10^3 cells/well in 100 μL of culture medium in 96-well plates, and grown overnight. After 24 hours incubation with different concentrations (0, 10, 25, 50, 100, or 200 μg/mL) of each nanoparticle, 20 uL of XTT was added. After 3 hours incubation, the absorbance (at 490 nm) of each well was measured by a microplate reader (Victor3). The relative cell viability (%) for each sample related to the control well was calculated. Each sample was tested in quadruplicate.

Cellular uptake of NPs. MCF-7 cells were seeded in a 35 mm glass-bottom culture dish (MatTek Corporation, Ashland, MA) at a density of 4 x 10^5 cells/well and incubated for 24 hours. The cells were treated with one type of nanoparticle (either **CPP0-Co**, **CPP0-Fe**, **PEG/CPP0-Fe** or **ANF/CPP0-Fe** at 100 μg/mL), and then incubated for 24 hours at 37 °C.

Prior to imaging, the cell membranes and nuclei were stained with Cell Mask™ Deep Red and Hoechst (Invitrogen), respectively, for 10 minutes. Fluorescence imaging was performed on a Leica TCS SP5 confocal fluorescence microscope.

The intracellular accumulation of **ANF/CPP0-Fe** was also quantified by fluorescence. Before the cell uptake experiments, MCF-7 cells were plated into six-well plates at a density of 4 x 10^5 cells/well and incubated overnight. The medium from each well was replaced with 1 mL of medium containing **ANF/CPP0-Fe** nanoparticles. After 24 hours of nanoparticle exposure, the medium was removed, and the attached cells were washed and trypsinized, and the cell pellets were lysed with PBS 1% SDS. The lysates were analyzed in a Jasco FP-8200 spectrofluorometer (excitation: 490 nm; emission: 520 nm). Cellular uptake (%) was calculated from the ratio of fluorescein concentration after treatment to that before treatment.

Anticancer activity of CPT@CPP0-Fe nanoparticles. The anticancer activity of **CPT@CPP0-Fe** nanoparticles was measured by the XTT assay using free CPT as a control . After incubating MCF-7 breast cancer cells with free CPT or **CPT@CPP0-**Fe nanoparticles (1, 2.5, 5, 7.5, 10, 25, 50 and 100 ng/mL) for 24 or 72h, 20 uL of XTT was added. After 3 h incubation, the cell viability was quantified using a microplate reader (Victor3). For IC50 calculations, survival data were evaluated by variable slope curve-fitting using Prism 4.0 software (GraphPad, San Diego, CA).

Acknowledgements

We acknowledge the financial support of the Ministerio de Economía y Competitividad through project MAT2012–38318-C03–02. F.N. thanks the Ministerio de Economía y Competitividad (MINECO) for a JdC (JCI-2011–09239) post-doctoral grant. F. N. thanks the Universidad Nacional del Sur for financial support. Thanks to COST Action MP1106 and TD1004.

References

[1] S. R. Batten, N. R. Champness, X. M. Chen, J. Garcia-Martinez, S. Kitagawa, L. Öhrström, M. O'Keeffe, M. P. Suhh, J. Reedijk, *CrystEngComm* **2012**, *14*, 3001–3004.

[2] a) M. Y. Masoomia, A. Morsali, *RSC Adv.*, **2013**, *3*, 19191-19218; b) X. Wang, R. McHale, *Macromol. Rapid. Commun.* **2010**, *31*, 331-350; c) W. Lin, W. J. Rieter, K. M. Taylor, *Angew. Chem. Int. Ed.* **2009**, *48*, 650-658; d) A. Spokoyny, D. Kim, A. Sumrein, C. A. Mirkin, *Chem. Soc. Rev.* **2009**, *38*, 1218-1227; e) V. A. Friese, D. G. Kurth, *Coord. Chem. Rev.* **2008**, *252*, 199-211.

[3] a) S. Kitagawa, R. Kitaura, S.-I. Noro, *Angew. Chem., Int. Ed.* **2004**, *43*, 2334-2375; b) G. Ferey, C. Serre, *Chem. Soc. Rev.* **2009**, *38*, 1380-1399; c) P. Horcajada, R. Gref,

T. Baati, P. K. Allan, G. Maurin, P. Couvreur, G. Ferey, R. E. Morris, C. Serre, *Chem. Rev.* **2012**, *112*, 1232–1268.

[4] a) M. Oh, C. A. Mirkin, *Nature* 2005, *438*, 651-654; b) X. Sun, S. Dong, E. Wang, *J. Am. Chem. Soc.* **2005**, *127*, 13102-13103.

[5] a) I. Imaz, J. Hernando, D. Ruiz-Molina, D. Maspoch, *Angew. Chem. Int. Ed.* **2009**, *48*, 2325-2329; b) S. Xu, L. You, P. Zhang, Y. Zhang, J. Guo, C. Wang, *Chem. Commun*. **2013**, *49*, 2427-2429; c) P. F. Gao, L. L. Zheng, L. J. Liang, X. X. Yang, Y. F. Li, C. Z. Huang, *J. Mater. Chem. B*, **2013**, *1*, 3202-3208; d) F. Freire, J. M. Seco, E. Quiñoá, R. Riguera, *J. Am. Chem. Soc*. **2012**, *134*, 19374-19383; e) C. Jo, H. J. Lee, M. Oh, *Adv. Mater*. **2011**, *23*, 1716-1719; f) R. Nishiyabu, C. Aimé, R. Gondo, T. Noguchi, N. Kimizuka, *Angew. Chem. Int. Ed. Engl*. **2009**, *48*, 9465-9468.

[6] a) H. Tan, C. Ma, Y. Song, F. Xu, S. Chen, L. Wang, *Biosensors and Bioelectronics* **2013**, *50*, 447-452; b) H. Tan, B. Liu, Y. Chen, *ACS Nano* **2012**, *6*, 10505-10511; c) C. Zong, X. Liu, H. Sun, G. Zhang, L. Lu, *J. Mat. Chem*. **2012**, *22*, 18418-18425; d) P. Huang, J. Mao, L. Yang, P. Yu, L. Mao, *Chem. Eur. J*. **2011**, *17*, 11390-11393.

[7] a) Y. Liu, Z. Tang, *Chem. Eur. J*. **2012**, *18*, 1030-1037; b) C. Aimé, R. Nishiyabu, R. Gondo, N. Kimizuka, *Chem. Eur. J.* **2010**, 16, 3604-3607; c) H. Wei, L. Y. Du, S. Dong, E. Wang, *Chem. Mater*. **2007**, *19*, 2987-2993.

[8] a) L. Amorín-Ferré, F. Busqué, J. L. Bourdelande, D. Ruiz-Molina, J. Hernando, F. Novio, *Chem. Eur. J.* **2013**, *19*, 17508 – 17516; b) L. Xing, H. Zheng, Y. Cao, S. Che, *Adv. Mater*. **2012**, *24*, 6433-6437; c) R. C. Huxford, K. E. deKrafft, W. S. Boyle, D. Liu, W. Lin, *Chem. Sci*. **2012**, *3*, 198-204; d) I. Imaz, M. Rubio-Martínez, L. García-Fernández, F. García, D. Ruiz-Molina, J. Hernando, V. Puntes, D. Maspoch, *Chem. Commun.* **2010**, *46*, 4737-4739; e) W. J. Rieter, K. M. Pott, M. L. Taylor, W. Lin, *J. Am. Chem. Soc*. **2008**, *130*, 11584-11585.

[9] a) F. Novio, J. Simmchen, N. Vázquez, L. Amorín, D. Ruiz-Molina, *Coord. Chem. Rev.* **2013**, 257, 2839– 2847; b) J. Della Rocca, D. Liu, W. Lin, *Acc. Chem. Res.* **2011**, 44, 957-968. c) J. Della Rocca, W. Lin, *Eur. J. Inorg. Chem.* **2010**, 3725-3734.

[10] a) R. A. Sperling, W. J. Parak, *Philos. Trans. R. Soc.* **2010***, 368,* 1333-1383; b) P. M. Tiwari, K. Vig, V. A. Dennis, S. R. Singh, *Nanomaterials* **2011**, *1*, 31-63.

[11] C. Amiens, B. Chaudret, D. Ciuculescu-Pradines, V. Colliere, K. Fajerwerg, P. Fau, M. Kahn, A. Maisonnat, K. Soulantica, K. Philippot, *New J. Chem.,* **2013**, *37*, 3374-3401.

[12] a) S. M. Cohen, *Chem. Rev.* **2012**, *112*, 970–1000; b) K. M. L. Taylor-Pashow, J. Della Rocca, Z. Xie, S. Tran, W. Lin, *J. Am. Chem. Soc*. **2009**, *131*, 14261–14263.

[13] a) C.-M. J. Hu, R. H. Fang, B. T. Luk, L. Zhang, *Nanoscale*, **2014**, *6*, 65-75; b) N. Sanvicens, M. P. Marco, *Trends Biotechnol.* 2008, 26, 425–433.

[14] K. Cho, X. Wang, S. Nie, Z. Chen, D. M. Shin, *Clin. Cancer Res.* **2008**, *14*, 1310-1316.

[15] a) H. Qu, D. Caruntu, H. Liu, C. J. O'Connor, *Langmuir* **2011**, *27*, 2271-2278; b) M. Lundqvist, J. Stigler, G. Elia, I. Lynch, T. Cedervall, K. A. Dawson, *PNAS* **2008**, *105*, 14265-14570; c) S. Taira, D. Kaneko, K. Onuma, A. Miyazato, T. Hiroki, Y. Kawamura-Konishi, Y. Ichiyanagi, *Int. J. Inorg. Chem.* **2012**, *ID 439751*, 7 pp.

[16] a) L. Chen, J. M. Mccrate, J. C-M. Lee, H. Li, *Nanotechnology* **2011**, *22*, 105708, 10 pp; b) A. Albanese, P. S. Tang, W. C. W. Chan, *Annu. Rev. Biomed. Eng.* **2012**, *14*, 1-16.

[17] a) R. Wiwattanapatapee, B. Carreno-Gomez, N. Malik, R. Duncan, *Pharm. Res.* **2000**, *17*, 991-998; b) P. Kohle, J. Khandare, O. Pillai, S. Kannan, M. Lieh-Lai, R. M. Kannan, *Biomaterials* **2006**, *27*, 660-669.

[18] P. K. Dhal, F. H. Arnold *Macromolecules* **1992**, *25*, 7051-7059.

[19] I. Imaz, D. Maspoch, C. Rodriguez-Blanco, J. M. Perez-Falcon, J. Campo, D. Ruiz-Molina, *Angew. Chem. Int. Ed.* **2008**, *47*, 1857 –1860.

[20] a) L.-L. Liu, J.-J. Huang, X.-L. Wang, G.-C. Liu, S. Yang, H.-Y. Lin, *Inorg. Chim Acta* **2013**, *394*, 715–722; b) Z.-L. Wang, M.-X. Li, *Acta Cryst.* **2010**, *C66*, m311–m313; c) B.-Z. Li, Y.-Z. Peng, Y.-P. Zhang, B.-L. Li, Y. Zhang, *Acta Cryst.* **2004**, *C60*, m560-m562.

[21] a) F. Meng, G. H. M. Engbers, A. Gessner, R. H. Müller, J. Feijen, *J. Biomed. Mater. Res. A* **2004**, *70*, 97-106; b) F.-H. Meng, Artificial cells based on biodegradable polymersomes. *Ph.D. thesis*, University of Twente, **2003**.

Figure captions

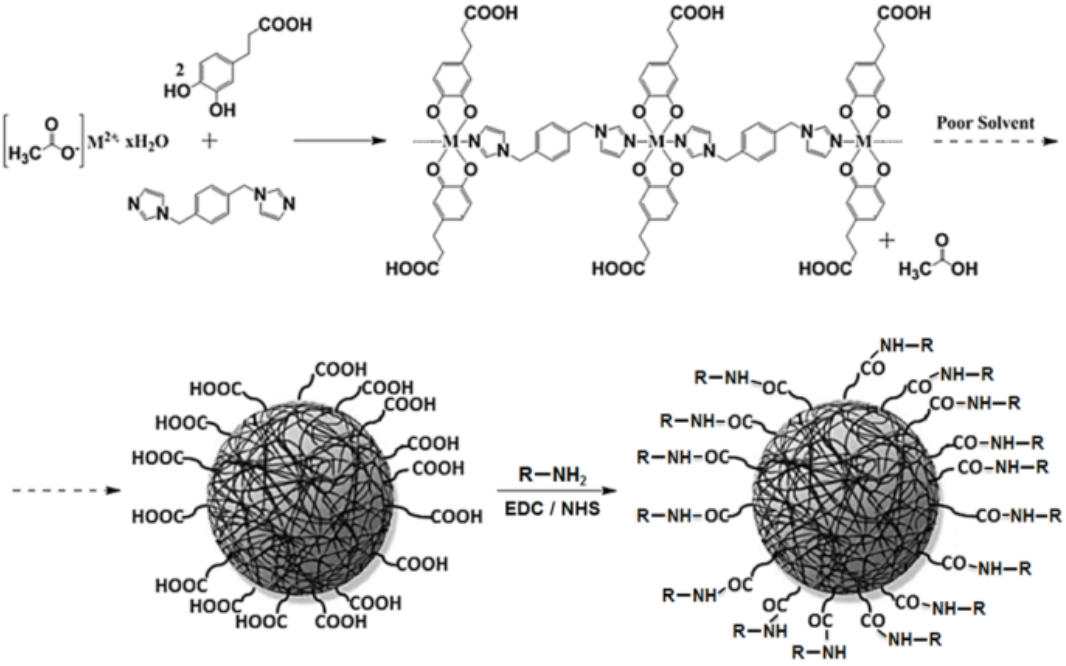

Figure 1. (Top) Schematic of the formation of polymeric chains and confinement into a nanostructure by fast precipitation. (Bottom) Schematic of the functionalization of nanoparticles containing carboxyl groups on the surface with different species containing amino groups mediated by carbodiimine coupling reaction.

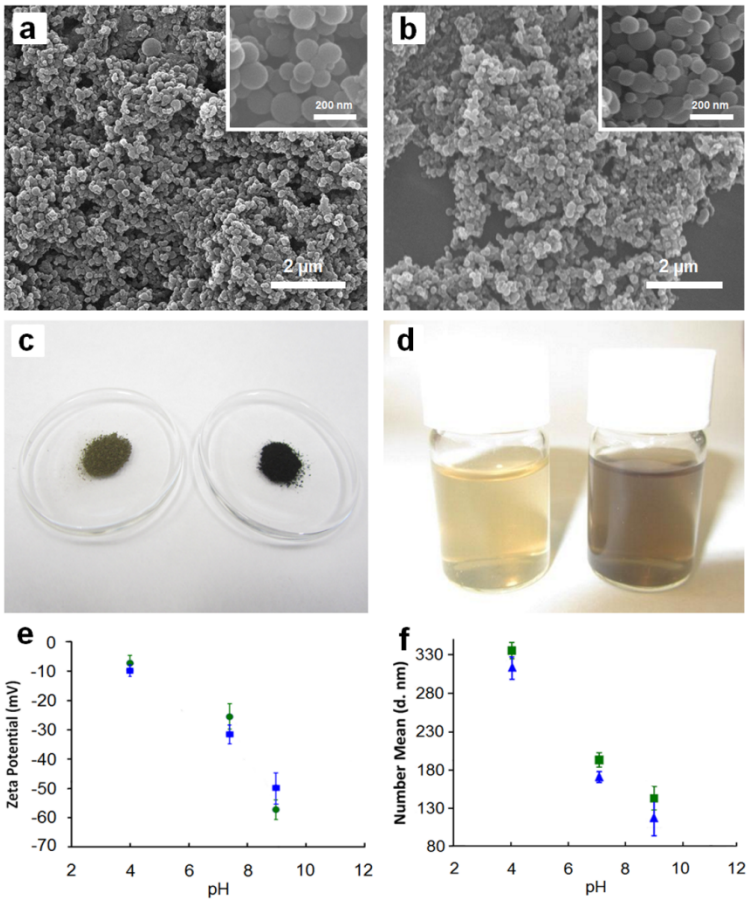

Figure 2. SEM images of a) **CPP0-Co** and b) **CPP0-Fe** nanoparticles showing good homogeneity and narrow size distribution; c) Solid samples and (d) water dispersions of **CPP0-Co** (pale brown) and **CPP0-Fe** (dark brown); e) Zeta-potential values for **CPP0-Co** (green dots) and **CPP0-Fe** (blue dots) at different pHs; f) DLS size dispersion measurements for **CPP0-Co** (green) and **CPP0-Fe** (blue) at different pHs.

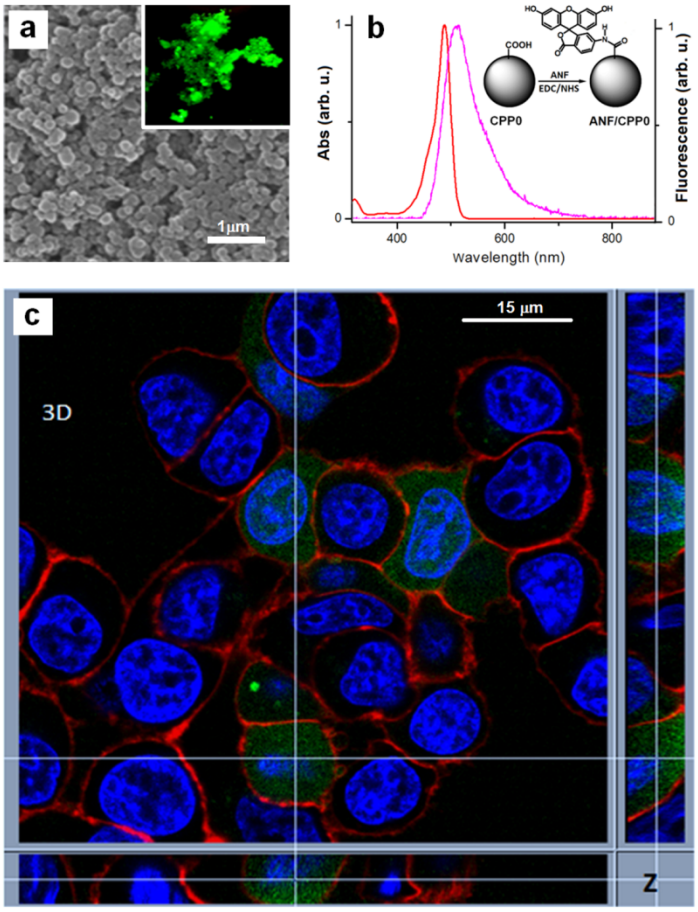

Figure 3. a) SEM image of **ANF/CPP0-Fe** nanoparticles (inset: image of fluorescence microscopy); b) Normalized absorption (red) and emission (pink) spectra for the 6-aminofluorescein attached to the **ANF/CPP0-Fe** surface; c) Confocal laser scanning microscopy images of the internalized fluorescent nanoparticles (**ANF/CPP0-Fe**).

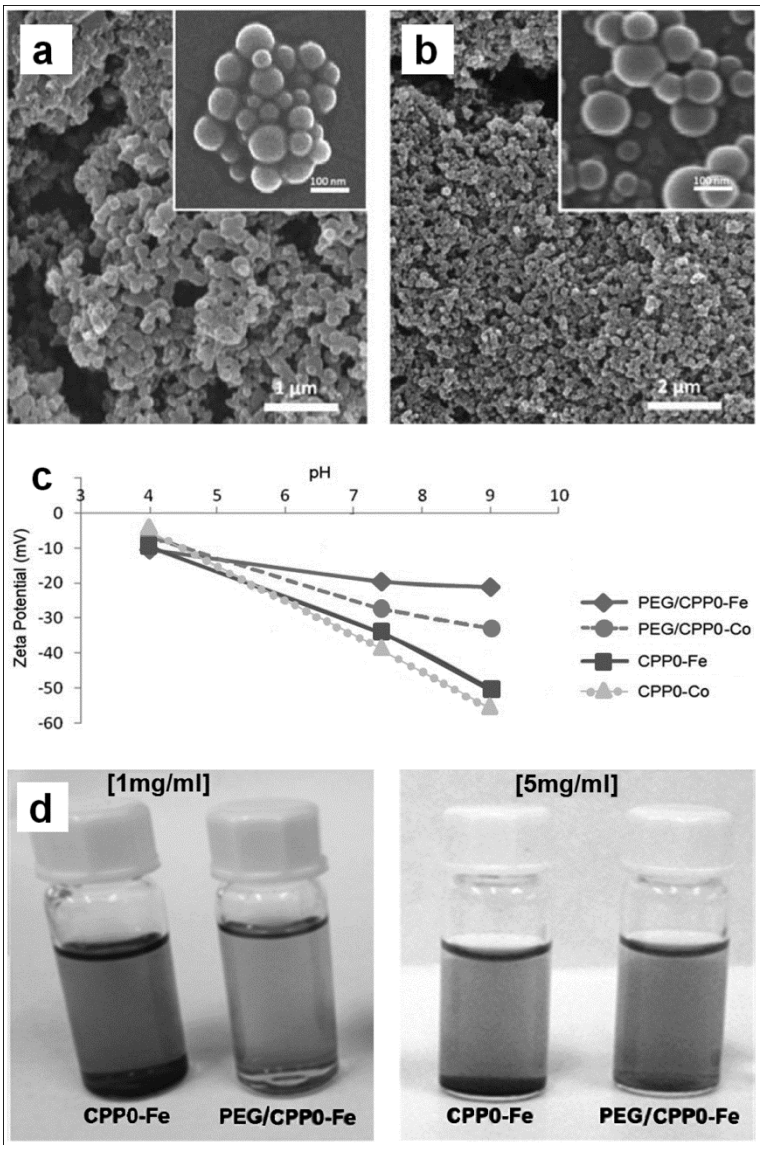

Figure 4. SEM images of **PEG/CPP0-Fe** (a) and (b) **PEG/CPP0-Co** nanoparticles; c) Zeta-potential measurements of the PEG-functionalized nanoparticles (**PEG/CPP0-Co** and **PEG/CPP0-Fe**) and the corresponding non-functionalized nanoparticles (**CPP0-Co** and **CPP0-Fe**). The decrease in free surface carboxylic groups after coupling with amino-PEG makes the zeta-potential less negative, and the value correlates to the concentration of PEG chains on the surface; d) Stability of colloidal dispersions of **CPP0-Fe** and **PEG/CPP0-Fe** at different concentrations in PBS after 1 week: 1mg/ml (left) and 5mg/ml(right). PEG is shown to improve the colloidal stability in PBS.

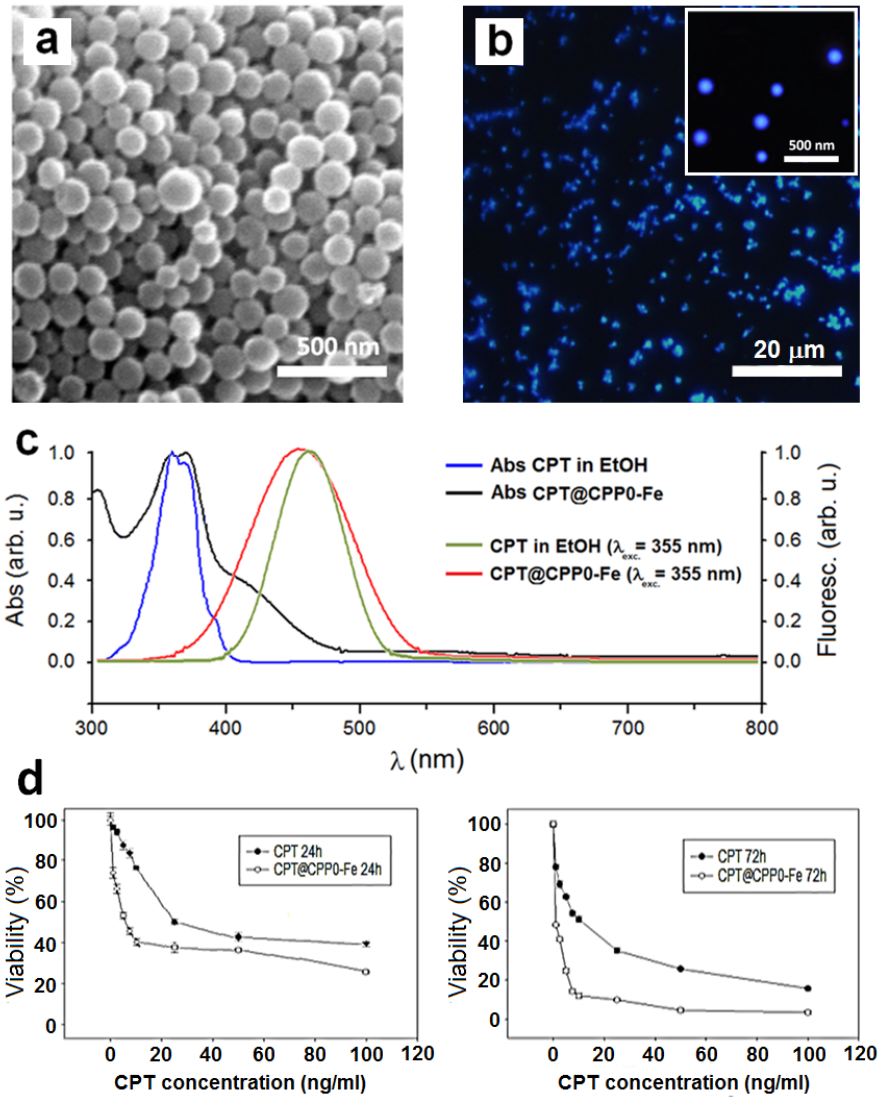

Figure 5. a) SEM image of **CPT@CPP0-Fe** nanoparticles; b) Fluorescence optical microscope images of **CPT@CPP0-Fe** spheres collected at λexc = 355 nm (inset: digital zoom image); c) Normalized absorption and emission spectra for CPT (absorption:blue/emission:green) and **CPT@CPP0-Fe** (absorption:black/emission:red); d) Cytotoxic effect of **CPT@CPP0-Fe** nanoparticles and comparison with free CPT at 24h (left) and 72h (right). Solid dots correspond to free drug and empty dots correspond to encapsulated CPT.

Text for the Table of Contents

Multifunctional CPPs: Robust and biocompatible coordination polymer nanoparticles with enhanced thermal and colloidal stabilities were obtained by incorporation of carboxyl groups on the amorphous structure. The surface carboxyl groups can be subsequently functionalized generating a multifunctional nanoplatform for theranostic applications (drug delivery & imaging).

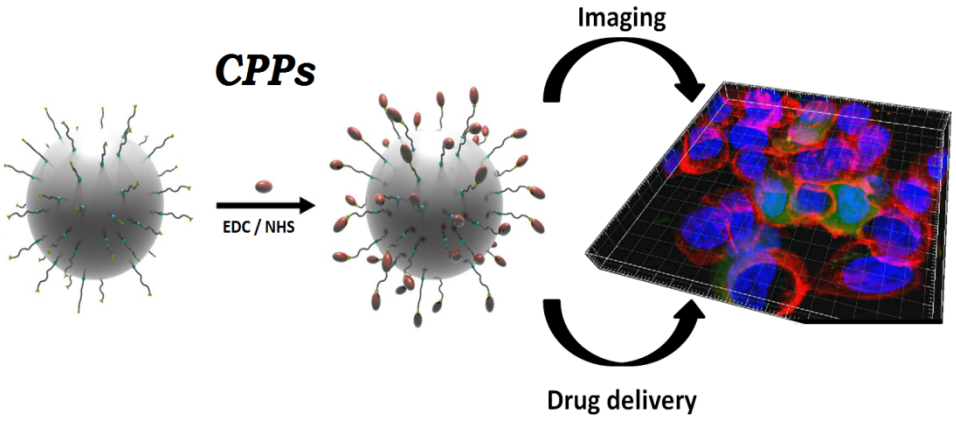

Keywords

Coordination polymer • nanoparticles • surface functionalization • drug delivery • catechol